EFDA–JET–PR(10)73

V. Petrzilka, J. Mailloux, J. Ongena, G. Corrigan, V. Fuchs, M. Goniche, V. Parail,
P. Belo, A. Ekedahl, P. Jacquet, M-L. Mayoral, C. Silva, M. Stamp
and JET EFDA contributors

# JET SOL Ionization at LH Wave Launching

# JET SOL Ionization at LH Wave Launching

V. Petrzilka[1], J. Mailloux[2], J. Ongena[3], G. Corrigan[2], V. Fuchs[1], M. Goniche[4], V. Parail[2], P. Belo[5], A. Ekedahl[4], P. Jacquet[2], M-L. Mayoral[2], C. Silva[5], M. Stamp[2] and JET EFDA contributors*

***JET-EFDA, Culham Science Centre, OX14 3DB, Abingdon, UK***

*[1]Association EURATOM-IPP.CR, Za Slovankou 3, 182 21 Praha 8, Czech Republic*
*[2]Association EURATOM-CCFE, Culham Science Centre, Abingdon, OXON OX14 3DB, UK*
*[3]Plasma Physics Laboratory, Royal Military Academy, Association EURATOM - Belgian State, Brussels, Belgium, TEC Partner*
*[4]Association EURATOM-CEA-Cadarache, IRFM, 13108 Saint Paul-lez-Durance, France*
*[5]Association Euratom-IST, Centro de Fusão Nuclear, Lisboa, Portugal*
** See annex of F. Romanelli et al, "Overview of JET Results", (23rd IAEA Fusion Energy Conference, Daejon, Republic of Korea (2010)).*

Preprint of Paper to be submitted for publication in
Plasma Physics and Controlled Fusion

**ABSTRACT.**
We present in this paper modeling of the JET Scrape-Off-Layer (SOL) including direct SOL ionization by launched LH (Lower Hybrid) waves. For that purpose, the two dimensional fluid code EDGE2D-NIMBUS was modified in order to account for possible enhanced ionization in the SOL due to the LH power absorbed by the electrons in a layer extending in the radial direction from the launcher. By taking the direct LH SOL ionization into account, the observed modification of the density in front of the LH antenna during LH power and gas injection can be explained. The JET grill private SOL limiters acting as sinks for the particles are also included in the model. We compare the efficiency of gas puffing from the Top and the Outer Mid-plane (OMP) for SOL density enhancement and improvement in LH coupling. The observed reduction of the temporal variation of the LH wave reflection coefficient and of measured saturated currents in the SOL during ELMs is explained. The density depletion by ponderomotive forces in front of the grill is estimated.

## 1. INTRODUCTION

Gas puffing with the JET gas inlet module 6 (GIM6) situated near the Lower Hybrid (LH) antenna increases the Scrape-Off Layer (SOL) electron density $n_{e,SOL}$ in the region magnetically connected to it, which improves the LH wave coupling [1], [2]. This is especially important for ITER where a large distance between the separatrix and the LH grill mouth is foreseen, which is likely to result in an electron density in front of the grill lower than the minimum required for good coupling of the LH wave. Numerical modeling with the fluid code EDGE-2D [3] suggested that enhanced edge radial plasma transport [4] can play a role in the SOL density increase, but agreement with the measured profiles could only be obtained using ad hoc modifications in the transport. The modeling did not take into account direct ionization by the LH wave, which is thought to contribute [1] to the density increase, either because of the SOL heating by collisional dissipation of the LH wave, or due to the fast electrons created by the LH wave parasitically in front of the grill mouth [5,6,7–12], or both. The process of parasitic dissipation and related fast electron production in front of the grill mouth is still not well understood. Recent experimental results from retarding field analyzer (RFA) measurements on Tore Supra [9,10] as well as from JET hot spot observations [12] have shown the existence of fast electrons as far as a few centimeters from the lower hybrid grill mouth. This finding contradicts earlier particle-in-cell simulation results [11], which predict interaction zones of the order of up to about 5mm.

In general, measurements reveal the presence of two electron components: the “cold” background plus a “hot” contribution corresponding to the fast electrons. The observed fast electrons causing hot spots can be divided into two distinct classes according to their temporal behavior [9,10]. To the first class belong fast electrons generated very close to the grill, characterized by Retarding Field Analyzer (RFA) collector signals, which persist during the application of the LH power. The second class of electrons causing hot spots on target components further away from the grill mouth - of the order of a few cm – exhibit temporal intermittency at a rate comparable with the detachment rate of relatively hot and dense plasma filaments, “blobs”, from the main body of the plasma. These blobs,

driven by the interchange instability, are ejected across the Last Closed Flux Surface (LCFS) around the mid-plane from the low field side of the torus and are observed, in experiment as well as in simulations, to move radially outward into the SOL, maintaining a radial extent of typically 1-2cm. As a blob moves radially outwards, simultaneously extending in the parallel direction along magnetic field lines, its temperature and density gradually decreases. This decrease is however slower than the temperature and density decrease of the background plasma into which the blob propagates. This essentially leaves a tenuous and relatively cold SOL between blob events. If under such conditions the background density exceeds the slow wave critical coupling value ($n_e = 1.7\times10^{17}$ $m^{-3}$ for $f_{LH}$ = 3.7GHz), the wave will propagate inward and experience very weak damping. It is only when the wave encounters a relatively dense and hot incoming blob, that the damping becomes appreciable. A novel theory of parasitic wave dissipation in front of the grill in a several cm wide layer in front of the grill mouth is presented in [27].

Experiments indicate that between 1% (Tore Supra) [5] and 20% (TdeV) of the LH energy can be lost in the SOL [7]. The high value for the lost power in TdeV was found for very high electron density at the grill mouth ($4.5\times10^{18}$ $m^{-3}$). The electron density in front of the grill in JET does not usually reach such high values, based on existing SOL measurements. If we believe that the fraction of power lost in JET to the fast electrons behaves as in TdeV and Tore Supra, (and the experimental observations from JET up to now do support this, at least qualitatively), then the maximum fraction of power lost will be much less than the high TdeV values in the type of experiments we are modeling.

Because of the lack of a complete theory for the parasitic dissipation of LH power in front of the grill, we estimate in this paper the amount of LH power lost in the SOL in JET using the experimental scaling law derived in Tore Supra [5], $F_{//} = 0.44\, n^{1.15}\, T^{0.59} \langle E_{RF} \rangle^{1.7}$, where $F_{//}$ is the heat flux along the field lines in MW $m^{-2}$, n (respectively T) is the electron density (respectively temperature) in front of the antenna in $10^{18}$ $m^{-3}$ (respectively eV) and $\langle E_{RF} \rangle$ is the RF electric field, in kV $cm^{-1}$, averaged over the 32 waveguides of the Tore Supra C3 launcher at the antenna aperture. Figure 1 shows the amount of LH power lost in the SOL in JET predicted by this scaling for two values of the density in front of the antenna, $0.2\times10^{18}$ $m^{-3}$ (blue curve with diamond) and $0.5\times10^{18}$ $m^{-3}$ (magenta curve with squares), T = 25eV, and various launched powers between 0.5 – 5MW, with $L_r$ the width of the dissipation layer and $L_{pol}$ the poloidal height. In this calculation we assumed $L_r$ = 2cm, $L_{pol}$ = 1m corresponding to the JET launcher height.

In what follows, the value of the dissipated power in front of the grill is an input to the computations, and the resulting SOL ionization and SOL density variations are determined from the code.

The two-fluid code EDGE-2D is used to explore the effect of the SOL heating on the electron density in the SOL $n_{e,SOL}$. Since EDGE-2D is a two-dimensional code (in radial and poloidal directions, it ignores the toroidal coordinate), it is assumed that the ionization by the LH wave is produced due to the local SOL electron heating by the LH waves in a radially narrow belt near the separatrix, with a poloidal width corresponding to the LH grill height. The absorbed power is introduced as a fixed source in the electron fluid equation. The ionization is computed in the code

under the assumption that the electron velocity distribution is Maxwellian. Plasma flow to the first wall is recycled as neutral atoms via recombination. The behaviour of neutrals is described by the numerical code Nimbus, which is called by EDGE2D during the computations. Modifications to EDGE-2D were required to accommodate the rather large SOL widths of about 8 cm for selected shots. The density at the separatrix is one of the boundary conditions. The second boundary condition is the power flux value through the separatrix.

Most of the modeling presented in this paper is done for the Pulse No: 66972 [14], which is one of a series of similar shots in JET designed for LH hot spots measurements. For this shot, it was possible to create a wide computational grid in the Outer Mid-Plane (OMP).

In the second section of this paper, the modification of the density in front of the LH antenna during LH power and gas injection is explored and compared with experimental observations. Modelling of the private SOL in front of the grill by introducing limiter-like features into EDGE-2D is attempted in section 3. Section 4 explores the time evolution of the SOL density, temperature, and other parameters when switching on/off the LH power and near grill gas puff. In section 5, we present modeling results of the time evolution of the JET SOL density, ionization sources, neutral density and other parameters due to ELM events *and* direct SOL LH ionization. Section 6 deals with the ponderomotive density depletion in front of the JET LH grill. Finally, conclusions are given in section 7.

## 2. SOL DENSITY VARIATIONS DUE TO POWER ABSORPTION FROM THE LH WAVE AND RESULTING IONIZATION

In this section, we describe the modelling of modifications of the density in the flux tube in front of the LH antenna observed experimentally during LH power and gas puffing [13-15]. As explained in the introduction, the enhanced ionization is obtained by assuming that a fraction of the LH power, called $P_{abs}$, is absorbed by the electrons in a layer extending in the radial direction from the launcher position (actually the wall position in the code) to a radius located at a distance $d_{LW}$ from the launcher. The particle and heat diffusion coefficients were set to $0.1 m^2/s$ near the separatrix ($R-R_{sep} < 0.01m$) and $1\ m^2/s$ elsewhere in the SOL. The modeling was performed for Pulse No: 66972 [14]. From the computed electron density and temperature profiles, the $J_{sat}$ signal is reconstructed in order to compare with measurements. When $P_{abs} = 0$, a steep $J_{sat}$ profile is obtained through the entire SOL (figure 2). With $P_{LH} = 0.4$ resp. 1.6MW, we found good agreement between the computed and measured values $J_{sat}$ assuming $P_{abs} = 10$kW resp. 50kW, showing that the dissipated power in the edge is a constant fraction of the launched power. The code indicates that the $J_{sat}$ increase is due to the increase in both $n_e$ and $T_e$. It should be stressed that this fluid code just considers the heating of thermal electrons and the resulting enhanced ionization rate of the neutrals. No fast electron population, although it is known to exist, is explicitly included in the plasma description in the modeling.

When D is reduced from 1 to $0.3 m^2/s$ in the close SOL ( $0.03<R-R_{sep}<0.05m$), $J_{sat}$ is almost divided by 2 in this zone but the decrease of $J_{sat}$ is weaker in the plateau zone. The experimental $J_{sat}$ data indicate that the diffusion coefficient should lie between these two values (figure 3). With no

LH power dissipated in the SOL, no reasonable value of the diffusion coefficient can be found to be consistent with the very flat $J_{sat}$ profile in the far SOL. This conclusion is opposite to the one from early experiments (performed with $CD_4$ injection) for which the change in the profile of transport seems to offer the only mechanism by which the edge density modification (increase of density by a factor ~2) can be reproduced by EDGE2D [4].

As the radial profile of the LH wave dissipation in the boundary plasma was found to be up to 5-6 cm wide in recent experiments [9, 10], we will also explore the wider width of the SOL dissipation layer in the computations: we will consider a narrower layer of about 2 cm width, and then a wider one of about 7 cm width. Clearly, the narrower heating profile results in stronger ionization effects for the same amount of dissipated power. In the following sections, we will use alternatively both the narrow and the broader heating profiles.

Most of the results presented in this paper are obtained for the geometry and parameters of JET Pulse No: 66972. Note however that we performed EDGE2D modeling also for other shots, like e.g. JET Pulse No: 58667 with a long distance between the separatrix and the LH grill mouth. It is a discharge (JET Pulse No: 58667, LH heating 2.5MW, B = 3T, Ip ramp from 1.5 to 2.7MA) from an experimental session to study LH coupling at large distances between plasma and LH grill [2], exhibiting also hot spots on the divertor apron, caused by fast particles locally accelerated in front of the grill mouth [6]. For this discharge, SOL density and temperature data from Reciprocating Probe (RCP) measurements are available.

## 3. MODELING OF THE GRILL PRIVATE SOL BY INTRODUCTION OF SIDE GRILL LIMITERS IN THE 2D MODEL

In experiments, the LH grill mouth is typically either flush with the nearest limiters, or protrudes 1 or 2 cm, or is retracted behind the limiters into its so called “private SOL” up to about 3cm. When the grill is being retracted behind limiters, the measured coupling can very quickly deteriorate, as the density just in front of the grill mouth decreases. The 3D geometry with the nearby limiters is illustrated on the right-hand side of Fig.4. To explore separately the behavior of the plasma density in the LH grill private SOL (between the two adjacent limiters), and in the rest of the SOL plasma, a 3D model is required. However, it is possible to define a private SOL in 2D geometry in EDGE-2D by introducing limiter-like features in the code [17]. The limiters are modeled as spatially localized sinks, where the recombination is artificially strongly enhanced. The configuration is illustrated on the left-hand side of Fig.4. This allows to distinguish the grill private SOL from the outside modeling region also in 2D geometry. This makes it possible to investigate the impact of various parameters on the density in the private SOL plasma, and in the rest of the SOL, separately. The parameters varied in this investigation are the gas puffing rate, the poloidal location of the gas injection, the amount of LH power dissipated in the SOL ($P_{abs}$) and its radial location. A limitation of the 2D modelling is that the gas injection location is always magnetically connected to the LH grill private SOL, as is the location of the ‘RCP measurement’. Hence it is not possible to compare between connected and non-connected locations in the same simulation (although doing separately

cases with and without LH provides the comparison). Nevertheless, the inclusion of a private SOL in the 2D modelling allows at least a first insight in how the SOL density varies near limiters adjacent to an active LH grill.

Figure 5 then shows the SOL density in the LH private SOL as a function of the limiter boundary location. The heating profile illustrated on the right hand side of Fig.5 is used. The gas puff rate is $10^{22}$ el/s, and is situated near the Outer Mid-Plane (OMP) in the modelling, i.e. in a similar location to GIM6 in the experiment. Heating in front of the grill is $P_{abs}$ =150kW. Figure 6 shows SOL density exactly in the limiter sink (top figure) and at the RCP location (bottom figure), again as a function of the limiter boundary location. The gas puffing and $P_{abs}$ are the same as in Fig. 5.

Figure 7 shows SOL density $n_{e,SOL}$ in the OMP (upper figure) as a function of the heating and puff rates, with distance limiter – wall $d_{LW}$ = 4.75cm; on the bottom figure there are neutrals profiles in the OMP. Let us note that simultaneous application of heating and gas puffing tends to flatten the $n_{e,SOL}$ profile, as indicated e.g. by the cyan diamonds. This flattening of the far $n_{e,SOL}$ profile is also observed in experiments [18]. It can be demonstrated in the modeling that the flatness of the $n_{e,SOL}$ profile depends also on the assumed profile of the LH wave dissipation. The nearer to the grill the LH power is dissipated, the flatter the $n_{e,SOL}$ profile becomes. Figure 8 shows $n_{e,SOL}$ in the OMP in the grill private SOL, as a function of the gas injection location, with $d_{LW}$ = 1.25cm, and $P_{abs}$ = 150 kW. Both the gas puffing and the heating/ionisation are important for raising the density in the far SOL. The OMP seems to be the most efficient location for gas puffing, but the two other locations (near the RCP, and at the top) also result in an increase in $n_{e,SOL}$ when heating is added. This could be significant for ITER, where top gas injection is foreseen.

## 4. TRANSIENT PROCESSES AT SWITCHING ON AND -OFF THE LH POWER AND GAS PUFF

Shorter (less than about 10 ms) and longer (about 50ms) characteristic times for the SOL plasma density evolution in locations magnetically connected and not-connected to the LH launcher, are measured by frequency swept reflectometry on Tore Supra during LH power modulation. We realized that two characteristic times could also be present in the time evolution of various JET SOL plasma parameters. The time evolution of the SOL density, H-alpha intensity and flows when switching on/off the LH and near grill gas puff is explored in this section [20].

On Fig.9 and 10, we can see the plasma density changes at the JET OMP and at the RCP locations at switching on the LH field. The grill mouth is assumed to be at 8 centimeters from the separatrix, 1 cm retracted behind the limiters.

At switching on/off the LH power or the gas puffing, the plasma density reaches equilibrium after rather long characteristic time of 50–100ms. Further away from the separatrix, the equilibrium is reached in a much shorter characteristic time of about 10ms, than closer to the separatrix.

A similar temporal behavior is exhibited by the $H_{alpha}$ intensity, as shown in Fig.11. The SOL density rises on the start of LH in the presence of a constant gas puffing because of the direct LH ionization in the SOL. On Fig.12, we show the temporal behavior of the plasma density at switching

on of the gas puffing during the application of the LH power. When switching off the LH power (resp. gas puff) at constant gas injection (resp. LH power), the plasma density returns to its original profile (cf. Fig.9), faster in the region away from the separatrix, where the parasitic LH absorption and direct ionisation were taking place. The plasma flows and their temporal behavior can be seen on Fig. 13. The flow velocity is rather low in the region denoted by the arrow in Fig.13, what can perhaps explain the relative slower relaxation times in some parts of the SOL.

The SOL density evolution at switch on and off of the LH power was measured in JET with the Li-beam diagnostic and the edge reflectometry. These JET SOL density measurements can recover the longer SOL relaxation times of about 50-100ms due to ionization effects which is close to the longer characteristic time found in the modeling, but the shorter relaxation time of the order of ms or tens of ms found in the modeling for regions near to the wall was not measured. For the Li beam, this is obvious because of the rather large sampling time interval. This is also the case for the SOL reflectometry as this diagnostic is not (and can not be for reasonable safety factor q values) magnetically connected to the grill mouth.

## 5. SOL OSCILLATIONS WITH ELMS ARE DECREASING DUE TO SOL LH IONIZATION

It can be frequently observed that the LH reflection coefficient oscillates with the ELM frequency, as the SOL density varies with ELMs, cf. Fig.18. For the same reason, the measured $J_{sat}$ in SOL by the reciprocating probe (RCP) also oscillates. In this section we present a modeling study of the time evolution of the JET SOL due to ELM events *and* direct SOL LH ionization [21]. The LH wave increases the SOL density by direct ionization of the SOL due to parasitic LH wave energy absorption. Similarly, as also ELMs bring energy into the SOL, the SOL temperature is increased and the SOL ionization is enhanced. ELMs are modeled by a standard option available in EDGE2D, which consists in enhancing transiently the transport coefficients on the low field side in a region near the separatrix. In the computations presented, the diffusion coefficient D is five times enhanced for 5ms in the interval $-0.02 < R\text{-}R_{sep} < 0.04$m to simulate an ELM event. The diffusion coefficient is assumed to increase linearly between 0–2.5ms, and then it again returns to its previous value between 2.5 and 5ms. The initial value of D is chosen as 0.1 $m^2/s$ for $R\text{-}R_{sep} < 0.03$m, and $1 m^2/s$ for $R\text{-}R_{sep} > 0.03$m. To increase the ionization effects at a given dissipation level, we reduced the radial extent of the LH heating profile. The amount of the dissipated power was tuned to $P_{abs}$ =50kW in front of the grill to fit the $J_{sat}$ measurements without taking into account ELMs in the modeling [14]. We concentrate on a shot with a wide SOL (JET Pulse No: 66972) and other shots from the same experimental session. As the computations show, a large fraction of the SOL neutrals are ionized by the LH parasitic dissipation before the ELM arrives, so that any additional contribution to the ionization of the SOL due to ELMs can only be small, cf. Fig.14 for the ionization source without and with LH heating, and Fig.15 for the neutral density without and with LH heating. The time evolution during the first 6 ms is shown after the start of the ELM process.

The modeled $j_{sat}$ variations due to ELMs and LH ionization are shown in Fig. 16. It follows from

the modeling that the SOL saturation current $j_{sat}$ (and the plasma density) in the far SOL in front of the grill is higher during LH due to the direct LH SOL ionization, but the additional $j_{sat}$ variations corresponding to ELMs are lower in front of the LH grill, where the LH power is dissipated. The reduction of $j_{sat}$ variations with ELMs and corresponding reduction in the plasma density variations explains the reduction in variations of the LH wave reflection coefficient observed experimentally in ELMy plasmas, when the LH power is increased. The modeled $j_{sat}$ with LH power "on" is confined between the red curve with full circles and the black curve with full squares during ELMs. The blue dashed lines bound the region of the modeled $j_{sat}$ during ELMs without LH.

The measurements of $J_{sat}$ [14] are compared with modeling results in Fig.17. The RCP measurements are denoted by empty red squares. The modeled limiting curves during an ELM, the red curve with red full circles and the black curve with black full squares, fit better to experimental data by tuning the radial profile of the diffusion coefficient D [14]. Here we use a very simple step and ramp model of D, as described above.

We could not model the huge $J_{sat}$ spikes found in some discharges [14] by the fluid EDGE2D model used, as testing even larger transport enhancements during ELMs resulted in numerical problems. For comparison with experiments, the modeled $D_{alpha}$ line intensity was also integrated along the standard diagnostic vertical line of sight from the top of the machine to the outer divertor apron. However, the modeling does not reproduce well the measured $D_{alpha}$ amplitude even for a very low LH power. The measured maxima are significantly larger than the modeled ones, and the measured minima are lower than the modeled ones. A similar discrepancy is seen also for discharges without LH and a wide SOL. One could speculate that the ELM model used in EDGE2D is not sufficient for taking into account important kinetic ELM features necessary for a good description of $D_{alpha}$. Problems with comparison of modeled $D_{alpha}$ with experiments in JET Diagnostic Optimized Configuration (DOC) were reported also in [21]. It is obvious that further modeling efforts are needed in order to obtain a better agreement with the experimental $D_{alpha}$ signal during LH.

In conclusion of this section, we note that the modeled $J_{sat}$ is in a good agreement with the RCP measurements during LH on and ELMs. During application of LH power, the modeled $J_{sat}$ (Fig.16, 17) oscillations decreased in the far SOL, which is consistent with the variations in reflection coefficient shown in Fig.18. The LH power ionizes the SOL even before the ELM arrives, and thus there remains less neutrals for ionization and consequent density variations due to ELMs.

## 6. DENSITY VARIATIONS DUE TO PONDEROMOTIVE EFFECTS AND IONIZATION IN FRONT OF THE JET LH GRILL

In plasmas with low $n_{e,SOL}$ in JET, gas puffing is used to increase the density in front of the grill and decrease the Reflection Coefficient (RC) during the application of the LH power. With low or no gas puffing, i.e. without sufficient neutrals to ionize, the measured RC is observed to increase with the LH power, $P_{LH}$. As the reflection coefficient exhibits a minimum as a function of the density [28, 22], this increase in RC can be caused by a decrease of the SOL density $n_{e,SOL}$ just in front of the grill mouth, at least for initially low densities below the RC minimum as a function

of $n_{e,SOL}$ in front of the grill. For a sufficiently high initial SOL density, the additional increase in density due to ionization can also result in an increase in the reflection coefficient. Shots exhibiting an increase in RC with power are e.g. shots 36971, 66970. Similar increases in RC observed on ASDEX [22] and recently on Tore Supra [23], were explained by expulsion of the plasma from the grill mouth along magnetic field B-lines by ponderomotive forces of the launched LH wave [22, 24]. In order to explore the ponderomotive force effects on JET, ponderomotive forces were included in EDGE2D. In the momentum equation for the electron fluid, a net time averaged force [22, 24] acting on electrons due to the gradient in the LH field was included in EDGE2D. This force expels electrons away from the grill mouth, and the ions follow due to the ambipolar effects. The electric field of the LH wave and the corresponding ponderomotive force value is computed for each time step of the EDGE2D code, using the LH wave propagation code [22]. This value of the ponderomotive force is used by EDGE2D for the computation of the density profile in the next time step, and then the density profile is returned into the LH propagation code, etc. A new equilibrium taking into account ponderomotive force effects is reached usually after a time interval of about 50ms. A reduction of $n_{e,SOL}$ by ponderomotive force effects in front of the grill mouth [22–24], and enhancement of $n_{e,SOL}$ by direct LH SOL ionization [4] are thus taken into account. Let us note that the ponderomotive force [22, 24] is proportional to the negative value of the gradient of the square of the LH electric field intensity E, and that the density depletion explored in a stationary equilibrium depends only on the ratio of the ponderomotive potential $W \sim E^2$ and on the plasma temperature, not on the characteristic length L of the W or E decrease along the magneto-static field on the sides of the grill. This decrease was modeled as a linear decrease. We choose for modeling a series of similar shots with a wide SOL. For these shots, it was possible to create a sufficiently wide SOL in the code of up to about 8 cm in the OMP, for which the far SOL temperature is of the order of several eV, comparable to the ponderomotive potential. In agreement with this, the parasitic absorption is assumed to take place between 5 and 8 cm from the separatrix, with a maximum plateau between 6 and 7 cm. There, enhanced ionization takes place due to enhanced far SOL temperature by the local parasitic LH wave absorption. We use a narrower heating profile, to simulate stronger ionization effects at a given dissipation level.

The radial extension of the limiters is variable in the modeling: When the grill side limiters do not protrude from the wall, with their top aligned with the wall at 8 cm from the separatrix, the computed ponderomotive density depletion is found negligible. The density depletion due to the ponderomotive force is significant only when the side limiters are protruding in front of the launcher by a (radial) distance comparable to the distance over which the parasitic absorption takes place. It is assumed in all the computations presented here that the nearest grill limiters are protruding from the wall, with their top located 5 cm from the separatrix. It is particularly useful for this study to introduce 3D private SOL features into the 2D code, which of course can only bring qualitative results.

In the figures 19, 20, and 21 below, we show results for the JET Pulse No: 66972. The computed density depletion in front of the grill shows almost no dependence on L, when L was varied from about 10 to about 30cm, in agreement with the analytical results obtained for the stationary

equilibrium [22,24]. The ponderomotive density depletion was computed for various values of $P_{LH}$ and gas puffing rates. The blue (diamonds) line and black (squares) line curves (Fig.19) correspond to the case of a zero gas puffing and assuming no direct ionization by the LH wave. Including ponderomotive forces resulting from the LH power density 20 MW/m$^2$ (about 5 MW for the whole launcher), a strong density depletion in front of the grill is seen, as indicated by the black line. The red (triangles) curve shows the case assuming ionization on top of this. This illustrates clearly that including ionization reduces effects of ponderomotive forces. The green (circles) curve then shows the hypothetical case of a ten times higher ponderomotive forces combined with ionization. The average electric filed E computed in the code near the grill mouth is E ~ 2kV/cm. It decreases from the grill mouth in the direction of the separatrix. As the temperature increases in the same direction, the ponderomotive effects are most outspoken in a small zone of about 1 or 2cm in front of the grill mouth. It is clear that the ponderomotive force effects decrease the plasma density significantly in this case, which may lead to a deterioration of the LH coupling. For the case of the red curve (triangles), we assumed that the plasma is ionized directly by the LH wave, and that only $P_{abs}$ =150kW is parasitically absorbed in front of the grill mouth. The effect of the ponderomotive forces is much reduced and not sufficiently strong to decrease the density in front of the grill. A significant decrease of the density in this case can only be reproduced assuming a ponderomotive force that is about ten times larger as shown by the green (circles) curve.

Figure 20 show the effect on the density profile for various strength of ponderomotive forces in presence of ionization. The red (triangles) and green (circles) curve are taken over from Fig.19 to compare with the case when the ponderomotive forces are left out completely as shown by the blue curve (diamonds). Figure 21 finally shows additional effects of a gas puff ($5\times10^{21}$ el/s) in front of the grill to the cases considered in Fig.20. The blue (diamonds) curve shows the case without ponderomotive forces, while the black (rectangles) curve shows the case with ponderomotive forces. The red (triangles) curve then shows the effect assuming ten times larger ponderomotive forces. It is clear that including ionization the conclusion on the density depletion remains the same, only ponderomotive forces about ten times stronger than computed can expel the plasma from in front of the grill mouth.

Such a strong pondemorotive force could exist due to the fast electrons generated parasitically in front of the grill, leading to charge separation as they escape the flux tube in front of the grill, and hence to an electric field which in turns affects the ions [25]. The enhanced ponderomotive force due to the presence of fast particles needs to be taken into account in future modelling, although it is not yet clear how this can be implemented.

Higher $N_{//}$, necessary for the fast electron generation, can be produced in a layer that is several cm deep as a result of the scattering of the LH wave on local SOL density modulations. An illustration is given in Fig.22. This density modulation is produced by ponderomotive force effects in front of the grill mouth [26]. As is explained above, ponderomotive density modulation effects are less important, when direct LH ionization is taken into account. This also means when the density increase due to direct LH SOL ionization is strong, the nonlinear high harmonic generation and

consequent parasitic LH wave absorption due to non-linear fast electron generation in front of the grill mouth will be weaker. A detailed investigation of this effect is out of the scope of this paper.

## CONCLUSIONS AND DISCUSSION

Numerical modeling presented in this work includes direct SOL ionization by the LH wave. The modeling shows the importance of taking into account effects of the LH power lost in the SOL and resulting in ionization of the gas present in the SOL. It is assumed in the two fluid code used, that the SOL ionization by the LH wave results from the local SOL electron heating by the wave. The fraction of LH power lost in SOL increases the SOL electron temperature, which in turn increases ionisation in the SOL. The modelling shows variations of several SOL parameters due to the direct LH wave SOL ionization.

In addition to the modeling of the plasma density and of the ionization source, we also studied the results of variations of the gas puffing and of the SOL heating rate on the temperature. The increase in the SOL temperature is largest without gas puffing. When the gas puffing is accompanied by sufficient SOL heating, the SOL plasma density strongly increases, which can explain the observed improvement of the LH wave coupling. The modeled density increase due to SOL heating and gas puffing is consistent with the modeled SOL ionization source profiles, which for gas puffing and heating are strongly enhanced and extend into the far SOL, contrary to the case without heating and/or without the gas puffing.

Although outer mid-plane seems to be the best location for gas puffing, the other two puffing locations (near RCP, at the top) also give an increase in $n_{e,SOL}$ with heating. This could be important for ITER, where top gas puffing is assumed. The modeling shows the flattening of the far $n_{e,SOL}$ profile, which is observed in experiments [2,18].

At switching on/off the LH power, we find that further away from the separatrix, where the LH parasitic dissipation and corresponding local SOL heating takes place, the computed plasma density increases with time at the onset of the local LH wave ionization with a short characteristic time of less than about 10 ms. Closer to the separatrix, the plasma density approaches the new equilibrium with much longer characteristic times. The variations in the SOL plasma parameters at LH switching on/off are larger with a larger near grill gas puffing and also with larger variations of the LH power.

The modeled $J_{sat}$ features explain the observed reduction of the LH wave reflection coefficient oscillations during ELMs at enhanced LH power. In addition, some insight into the SOL ionization by the combined effect of ELMs and parasitic SOL LH wave dissipation was obtained: The LH ionizes the SOL even before the ELM arrives, and there remains less neutrals for ionization by the ELM.

We also note that without taking into account the gas ionization in front of the grill mouth, the computed density in front of the grill can decrease significantly due to the ponderomotive depletion for launched LH powers of about 5 MW (about 20 MW/m$^2$). However, the ponderomotive forces are not strong enough to expel the plasma from in front of the grill mouth, when the direct ionization by the LH wave is taken into account. Only for ponderomotive forces about ten times larger than

computed, the plasma density would decrease in front of the grill mouth even with the gas puff directly ionized there. Such strong expelling effects could be perhaps provided by fast electrons generated locally in front of the grill, which escape from the grill and create an electric field by charge separation, pushing ions away from the locations in front of the grill mouth [25]. The expelling effect of the fast particles needs to be accounted for in future modeling, but the way how to do this is yet obvious.

**ACKNOWLEDGEMENTS**

This work was supported by EURATOM and carried out within the framework of the European Fusion Development Agreement. The views and opinions expressed herein do not necessarily reflect those of the European Commission. V. Petrzilka and V. Fuchs acknowledge partial support by the Czech Science Foundation Projects GACR 202/07/0044 and 205/10/2055, and of MSMT CR Grant Project ID LG11018.

**REFERENCES**

[1]. Pericoli-Ridolfini V, Ekedahl A, Erents S K, Mailloux J, Podda S, Sarazin Y, A. Tuccillo A A and the EFDA-JET Workprogramme contributors 2004 *Plasma Physics and Controlled Fusion* **46** 349-368

[2]. Ekedahl A, Granucci G, Mailloux J, Baranov Y, Erents S K, Joffrin E, Litaudon X, Loarte A, Lomas P J, McDonald D C, Petrzilka V, Rantamaki K, Rimini F G, Silva C, Stamp M, Tuccillo A A and JET EFDA Contributors 2005 *Nuclear Fusion* **45** 351-359

[3]. Simonini R, Corrigan G, Radford G, Spence J and Taroni A 1994 *Contribution Plasma Physics* **34** 368-373

[4]. Matthews G F, Erents S K, Corrigan G, Fundamenski W, Garcia-Cortes I, Mailloux J, Hidalgo C, Pedrosa M A, Pericoli V, Spence J, Silva C, Strachan J and contributors to the EFDA-JET workprogramme 2002 *Plasma Physics and Controlled Fusion* **44** 689-695

[5]. Goniche M *et al* 1998 *Nuclear Fusion* **38** 919-937; 2004 *Plasma Physics and Controlled Fusion* **46** 899–923

[6]. Rantamaki K M, Petrzilka V, Andrew P. Coffey I, Ekedahl A, Erents K, Fuchs V, Goniche M, Granucci G, Joffrin E, Karttunen S J, Lomas P, Mailloux J, Mantsinen M, Mayoral M-L, McDonald D C, Noterdaeme J-M, Parail V, Tuccillo A A, Zacek F and Contributors to the EFDA—JET Workprogramme 2005 *Plasma Physics and Controlled Fusion* **47** 1101-8

[7]. Mailloux J et al 1997 *Journal of Nuclear Materials* **241-243** 745

[8]. Fuchs V *et al* 1996 *Physics of Plasmas* **3** 4023

[9]. Gunn J P, Petrzilka V, Ekedahl A, Fuchs V, Gauthier E, Goniche M, Kocan M, Pascal J Y and Saint-Laurent F 2009 *Journal of Nuclear Materials* **390-391**, 904-9

[10]. Gunn J P, Petrzilka V, Fuchs V, Ekedahl A, Goniche M, Hillairet J, Kocan M and Saint-Laurent F 2009 *Radio Frequency Power in Plasmas, AIP Conference Proceedings* **1187** 391-3

[11]. Rantamaki K M *et al* 2000 *Nuclear Fusion* **40** 1477-1485

[12]. Jacquet P *et al* 2009 *Radio Frequency Power in Plasmas, AIP Conference Proceedings* **1187** 205-7
[13]. Petrzilka V *et al* 2006 *Proc. of the 33rd EPS Conference on Plasma Phys. Rome* ECA Vol. **30I** P-1.067
[14]. Goniche M *et al* 2009 *Plasma Physics and Controlled Fusion* **51** 044002
[15]. Ekedahl A *et al* 2009 *Plasma Physics and Controlled Fusion* **51** 044001
[16]. Granucci G *et al* 2003 *30th EPS St. Petersburg* ECA **27A** P-1.191
[17]. Petrzilka V *et al* 2007 *34th EPS07 Conference Warszaw,* paper P4.100, preprint EFDA–JET–CP(07)03/60
[18]. Goniche M, Ekedahl A, Mailloux J, Petrzilka V, Rantamaki K, Delpech L, Erents K, Stamp M, Zastrow K D and JET EFDA contributors 2007 *34th EPS07 Conference, Warszaw,* paper P1. 152, preprint EFDA–JET–CP(07)03/40
[19]. Petrzilka V, Goniche M, Fuchs V, Clairet F, Corrigan G, Belo P, Ongena J and JET EFDA contributors 2008 *35th EPS Conference, Hersonissos, Crete, Greece,* paper P1.106, JET preprint EFD-C-08-0327
[20]. Petrzilka V, Corrigan G, Belo P, Ekedahl A, Goniche M, Jacquet P, Mailloux J, Ongena J, Mayoral M-L, Parail V and Zacek F 2009 *Proceedings of the 36th EPS Conf. on Plasma Physics, Sofia, Bulgaria* P5.166
[21]. Kallenbach A *et al* 2004 *Plasma Physics and Controlled Fusion* **46** 431-445
[22]. Petrzilka V et al 1991 Nuclear Fusion 31 1758-1767
[23]. Ekedahl A *et al* 2009 *Radio Frequency Power in Plasmas, AIP Conference Proceedings* **1187** 407-9
[24]. Petrzilka V *et al* 1983 J. Plasma Phys. **30** 211-219; Klima R 1966 Soviet Phys. JETP **23** 534-536
[25]. Petrzilka V *et al* 2000 *18th IAEA Conference, Sorrento* paper CN-77/EXP4/07
[26]. Petrzilka V, Fuchs V, Gunn J P, Ekedahl A, Goniche M, L. Krlin L, Pavlo P and Zacek F 2009 *36th EPS Conf. on Plasma Physics, Sofia,* paper P4.207
[27]. Fuchs V, Gunn J P, Petrzilka V, Horacek J, Seidl J, Ekedahl A, Goniche M and Hillairet J 2009 *Radio Frequency Power in Plasmas, AIP Conference Proceedings* **1187** 383-5; Petrzilka V, Fuchs V, Gunn J, Fedorczak N, Ekedahl A, Goniche M, Hillairet J and Pavlo P, *Plasma Physics and Controlled Fusion* **53** (2011) 054016 (11pp), doi:10.1088/0741-3335/53/5/054016
[28]. Petrzilka V, Corrigan G, Fuchs V, Ekedahl A, Goniche M, Jacquet P, Mailloux J, Mayoral M-L, Ongena J, Parail V, Modelling of the density modifications in front of the LH launcher during gas injection in ITER, *38th EPS Conference on Plasma Physics (2011), Strasbourg*, contribution P4.099
[28]. Stevens J E *et al* 1981 *Nuclear Fusion* **21** 1259

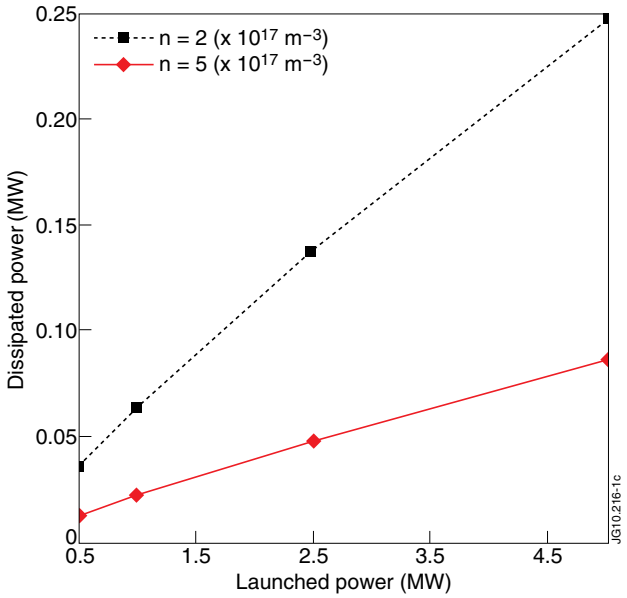


*Figure 1: Dissipated power in front of the grill according to the scaling law derived in [5].*

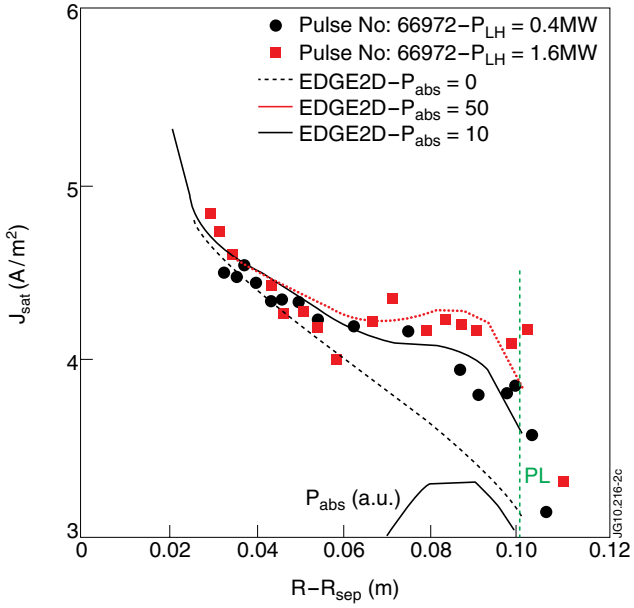


*Figure 2: Modeling of $J_{sat}$ (Pulse No: 66972) with $P_{abs}$ = 0 (dashed line) and $P_{abs}$ = 10 (blue line) and $P_{abs}$ = 50 (red line). $d_{LW}$ = 0.02m. Experimental data (after time averaging) for 2 LH powers are shown with closed circles. PL denotes the limiter position in the modeling.*

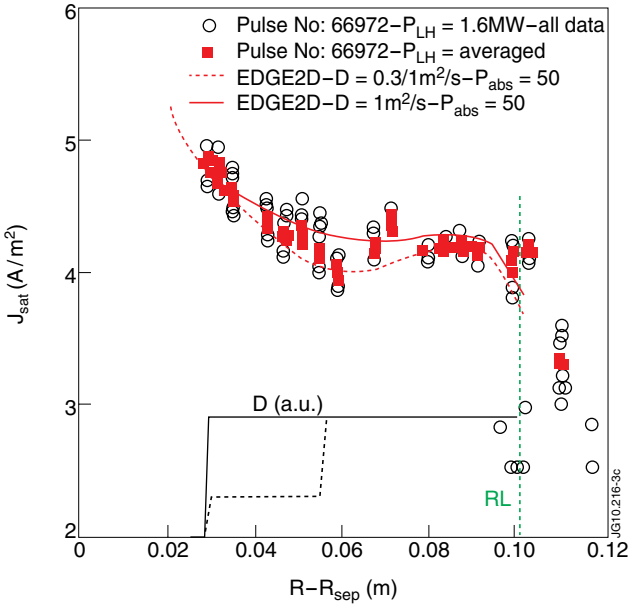


*Figure 3. Modeling of $J_{sat}$ (Pulse No: 66972) with two values of diffusion coefficients D = 0.3$m^2$/s and 1$m^2$/s in the region defined by 0.03m<R-$R_{sep}$<0.05m (D = 1$m^2$/s for R-$R_{sep}$> 0.055m). RL denotes the limiter position in the modeling.*

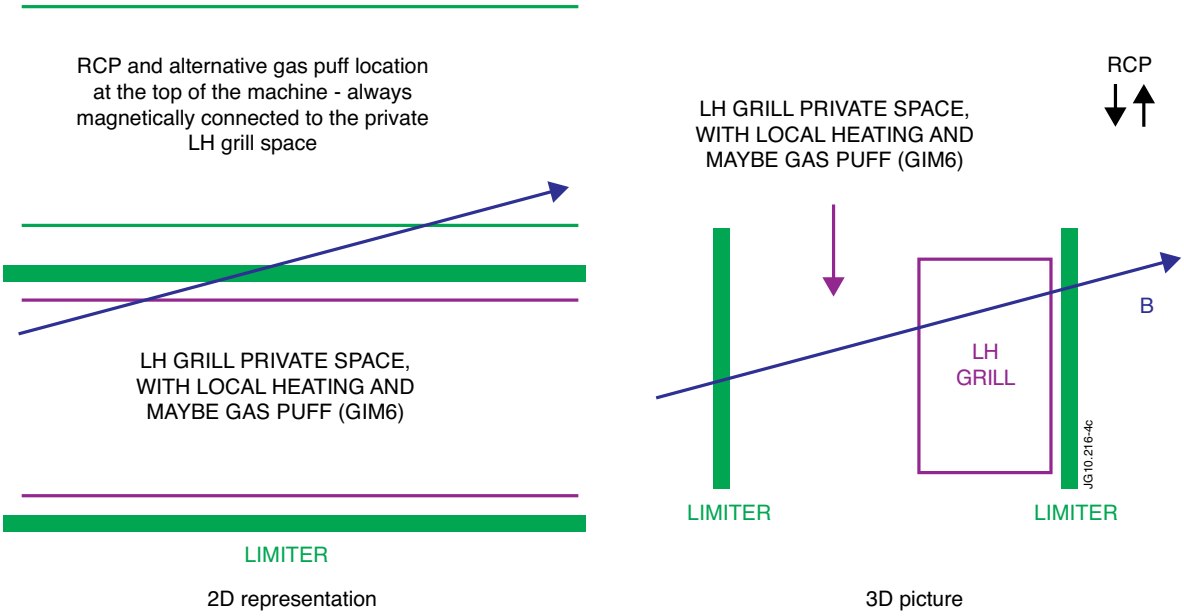


*Figure 4: Schematic representation of the 2D and 3D configuration of the LH grill and RCP.*

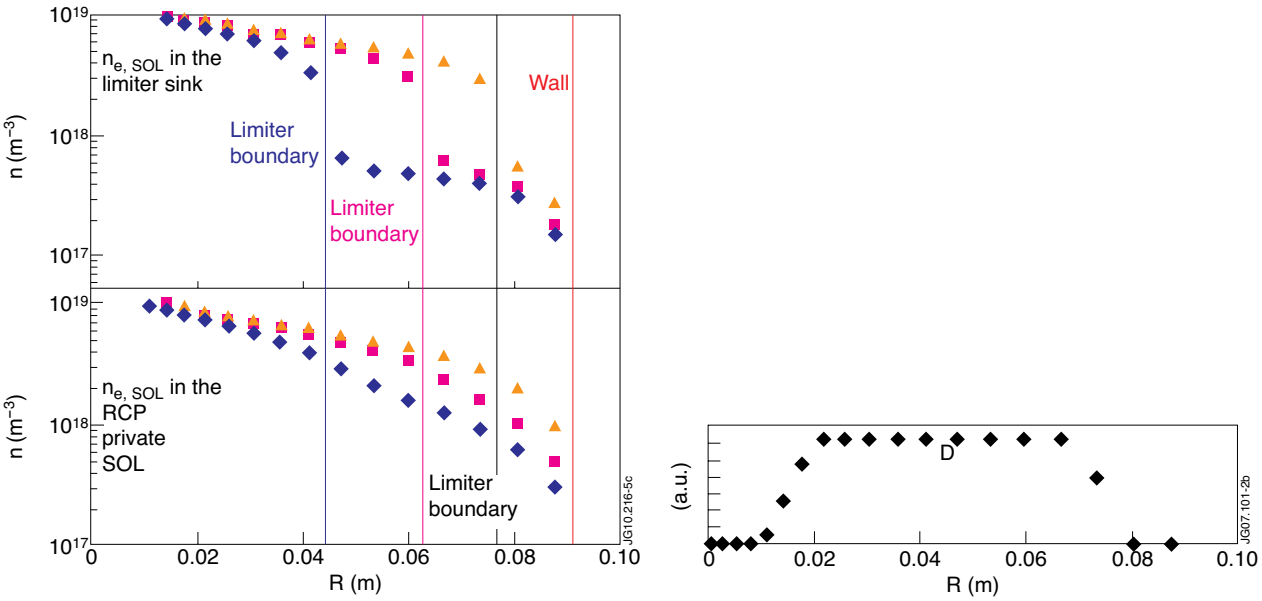


*Figure 5: Left figure: Effects of the limiter boundary location on the SOL density profile. x- axis: distance from separatrix in m. Series 1 (blue diamonds): distance limiter – wall in the modeling $d_{LW}$ =4.75cm (grill ~ 3 cm behind the limiter), series 2 (magenta rectangles): $d_{LW}$= 2.75cm (grill ~ 1 cm behind the limiter), and series 3 (yellow triangles): $d_{LW}$= 1.25cm (grill is ~ flush with the limiter). Right figure: Profile of the LH field dissipation (a.u.).*

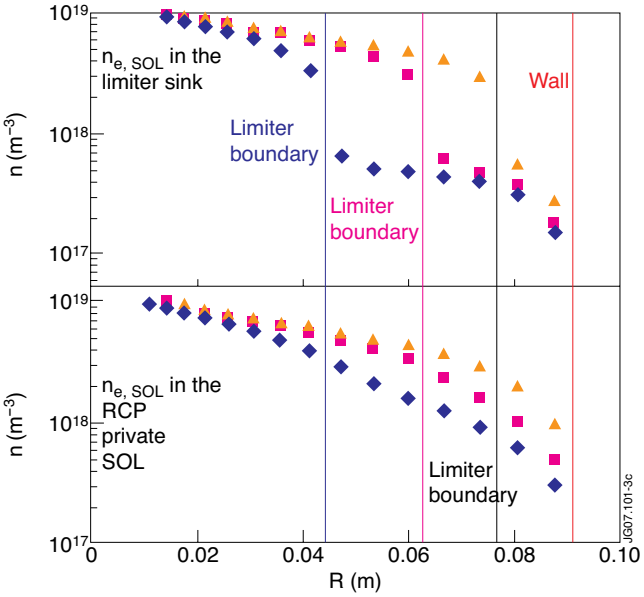


*Figure 6: Profiles of SOL density near limiters and in the RCP location, notation same as in Fig.5.*

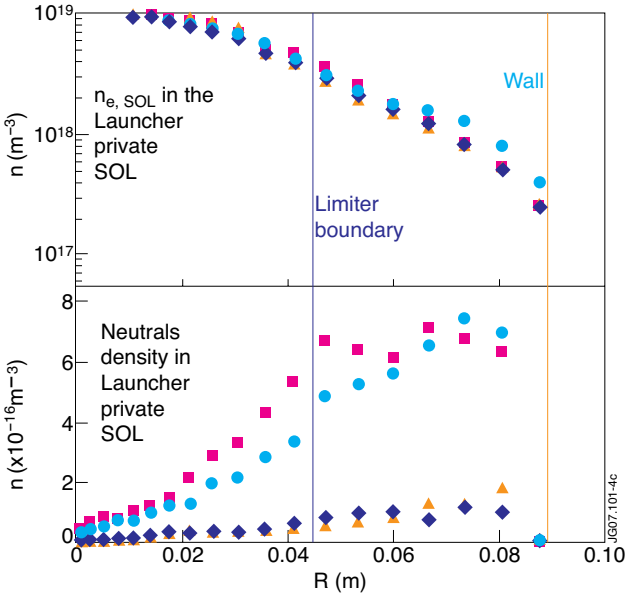


*Figure 7: Upper figure: SOL density as a function of the heating and puff rates. Bottom figure: corresponding neutrals profiles in the OMP. Blue diamonds: 0 heating, 0 puff, magenta rectangulars: 0 heating, puff = $10^{22}$ el/s, yellow triangles: heating $P_{abs}$ = 150kW, 0 puff, Cyan diamonds: heating $P_{abs}$ = 150kW, puff = $10^{22}$ el/s.*

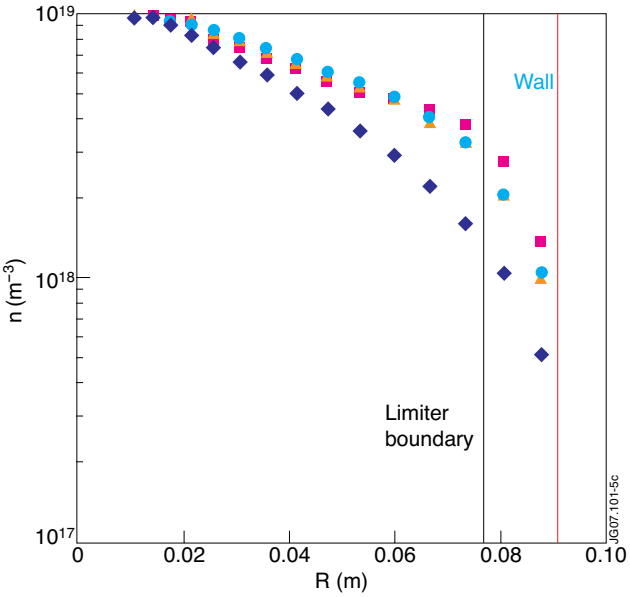


*Figure 8: Profile of the SOL density in the grill private SOL, as a function of the gas puff location. Blue diamonds: 0 heating, 0 puff, magenta squares: gas puff $10^{22}$ el/s near OMP, yellow triangles: gas puff near RCP, cyan diamonds: gas puff at the top.*

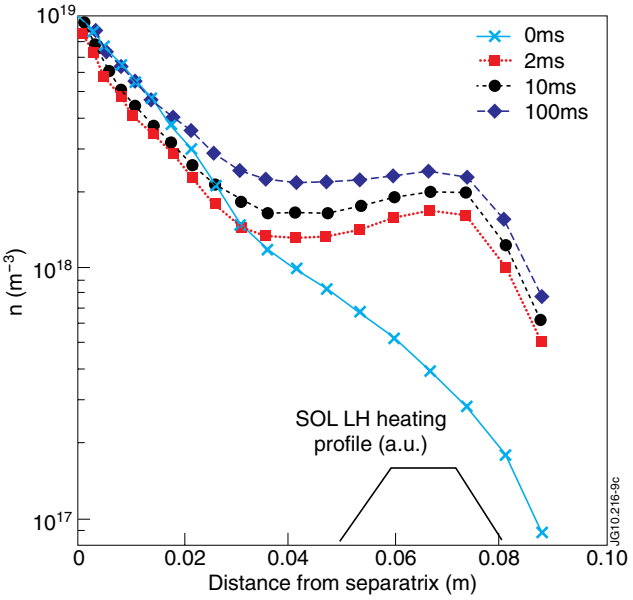


*Figure 9: OMP SOL plasma density at switching on the LH field: $P_{abs}$ =50kW dissipated in front of the grill, gas puff $10^{22}$ el/s.*

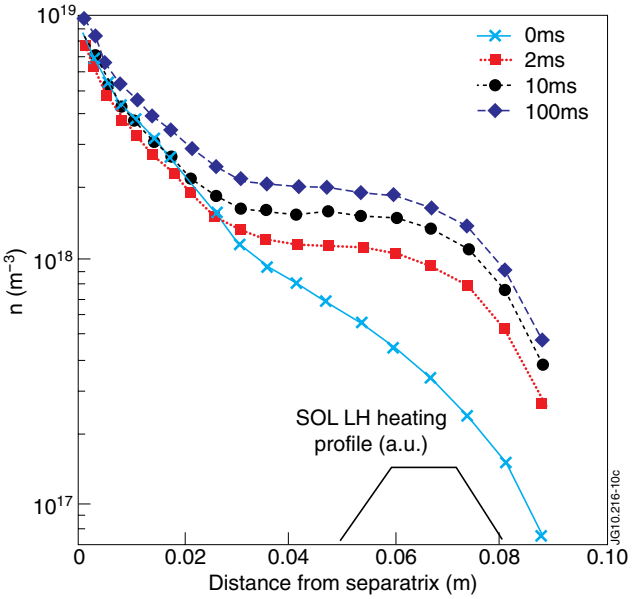


*Figure 10: RCP location plasma density at switching on the LH field: $P_{abs}$ = 50kW dissipated in front of the grill, gas puff $10^{22}$ el/s.*

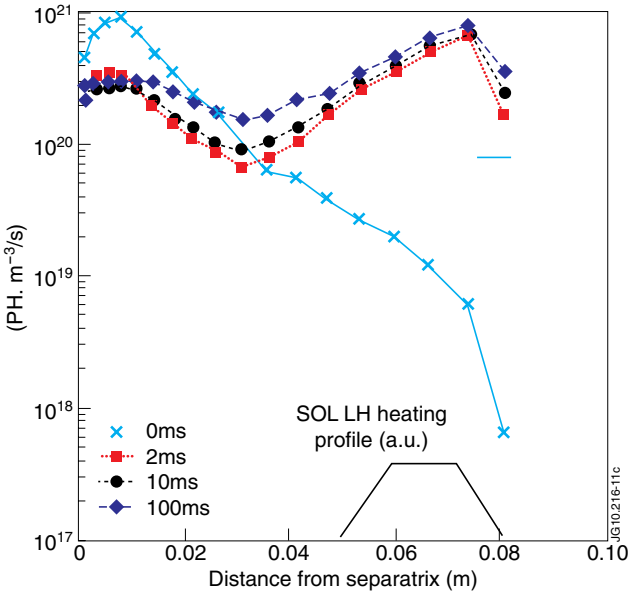


*Figure 11: OMP SOL H_alpha radiation intensity at switching on the LH field: $P_{abs}$ = 50kW dissipated in front of the grill, gas puff $10^{22}$ el/s*

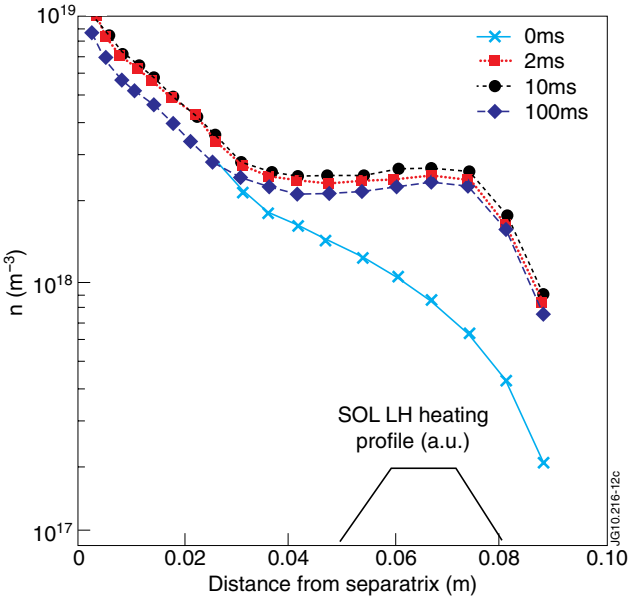


*Figure 12: OMP SOL plasma density at switching on the gas puff $10^{22}$ el/s; $P_{abs}$ = 50kW LH power dissipated in front of the grill.*

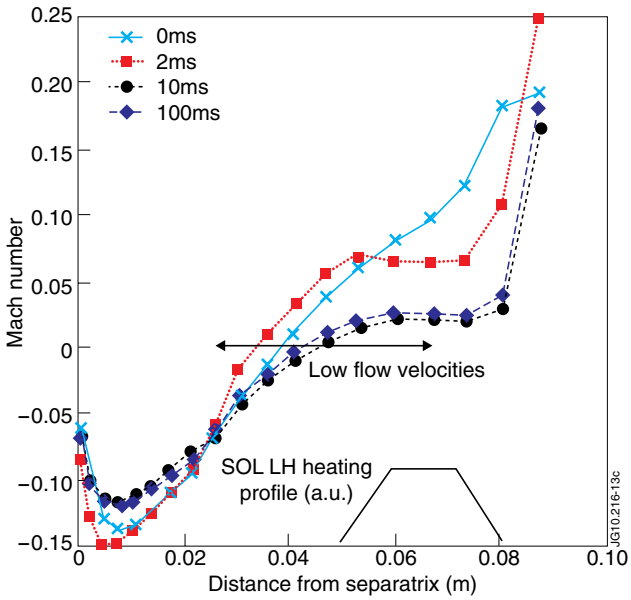


*Figure 13: Flow Mach number variations in SOL at switching on the gas puff 1e$^{22}$ el/s; LH field: $P_{abs}$ = 50kW dissipated in front of the grill.*

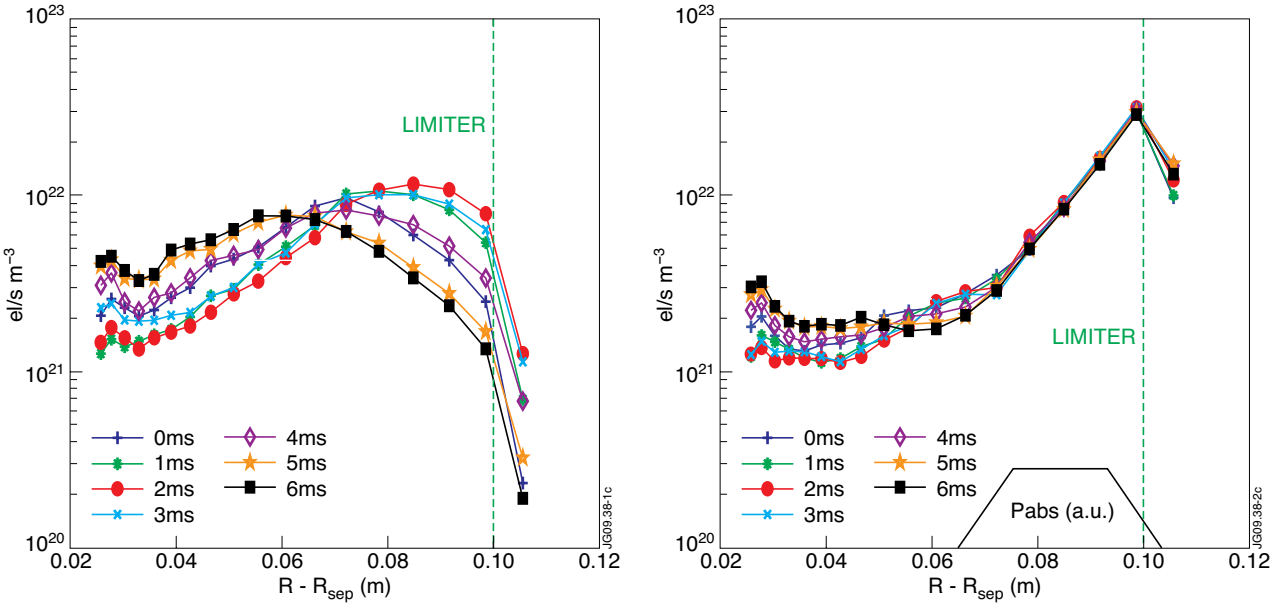


*Figure 14: Ionization source during an ELM in 1ms intervals, left: LH "off", right: LH "on".*

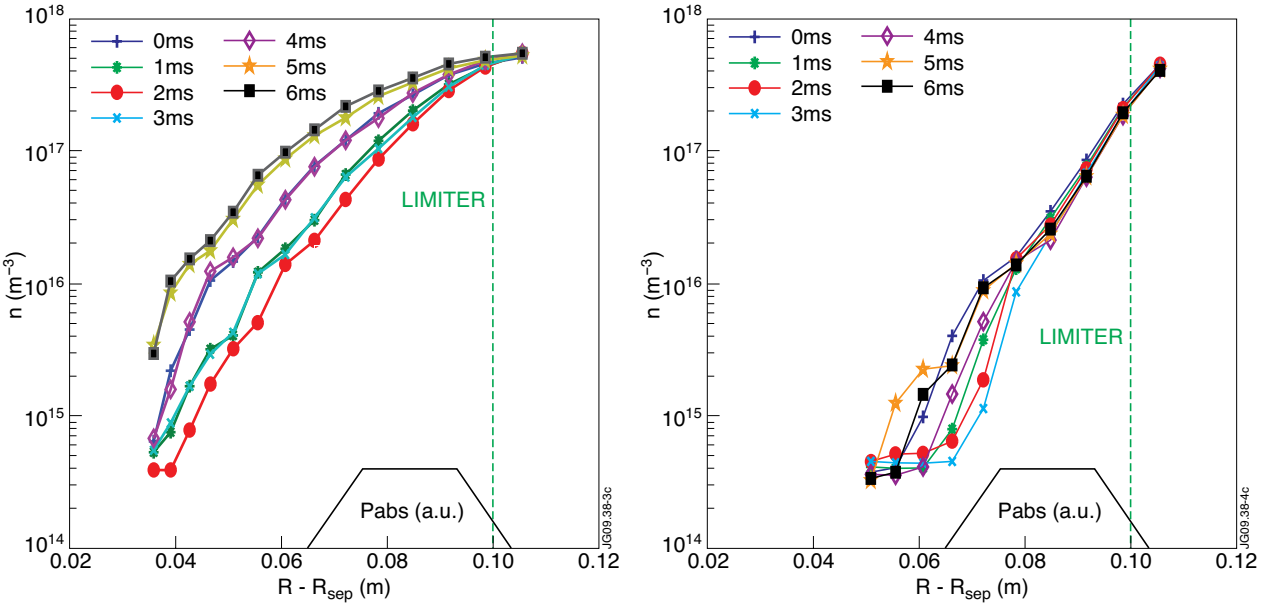


*Figure 15: Neutral molecule density during an ELM in 1 ms intervals, left -LH "off", right - LH "on".*

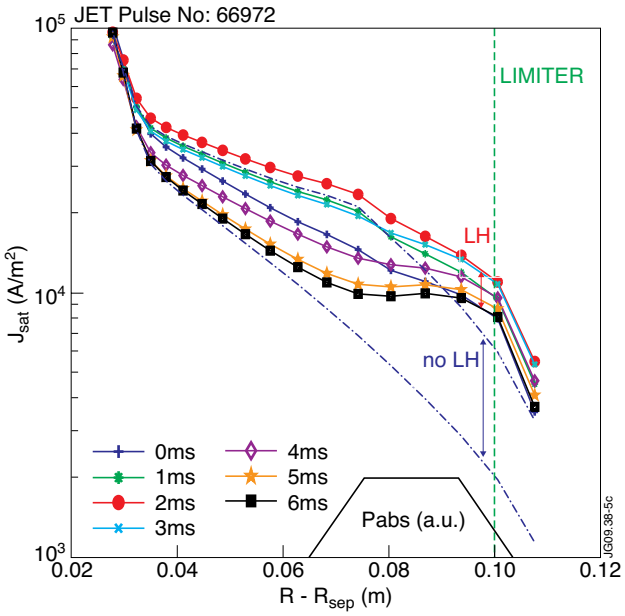


*Figure 16: Saturation current density jsat during an ELM in 1 ms intervals, LH on; and modeled saturation current density jsat limits during an ELM, LH "off" - blue curves, dash and dot.*

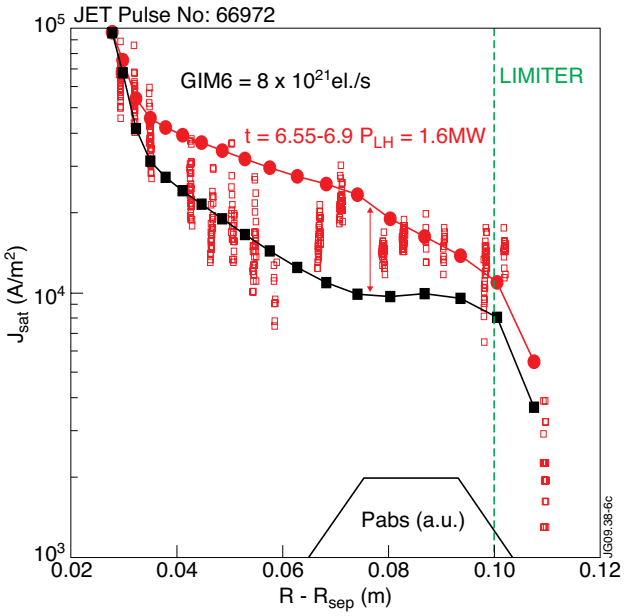


*Figure 17: Modeled saturation current $J_{sat}$ density limits during an ELM and LH "on" - red curve with red full circles and black curve with black full squares, measured data are represented by empty red squares [8].*

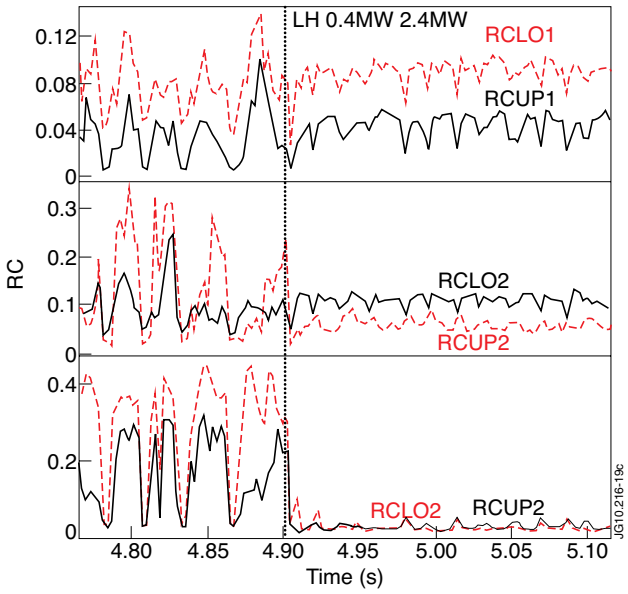


*Figure 18: The oscillations of the reflection coefficient RCLOi and RCUPi for JET Pulse No: 66971 in the lower and upper part of individual i = 1, 2, 3 rows decrease in ELMs with enhanced LH power from 0.4 to 2.4MW after time 4.90s, which is consistent with the decrease of $J_{sat}$ oscillations at LH on in Fig.17.*

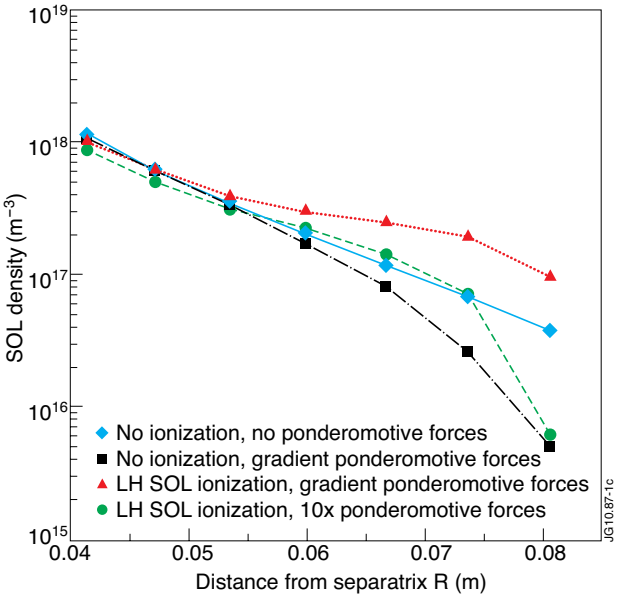


*Figure 19: Density depletion due to ponderomotive forces, no gas puff.*

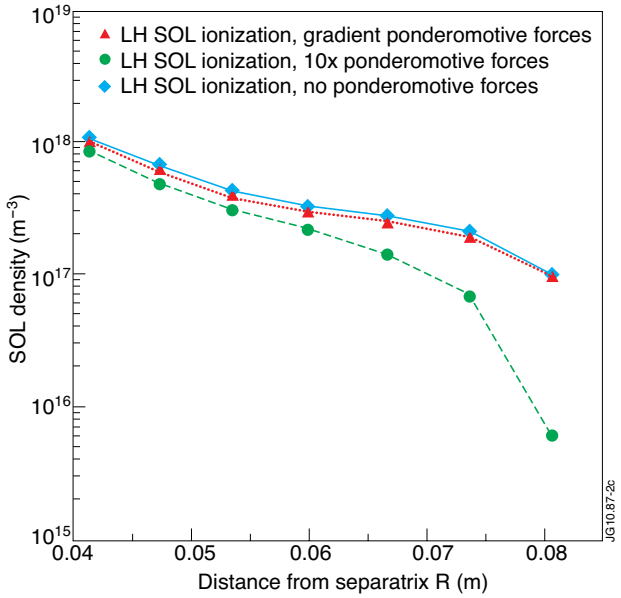


*Figure 20: Density depletion, ponderomotive forces, ionization, no gas puff.*

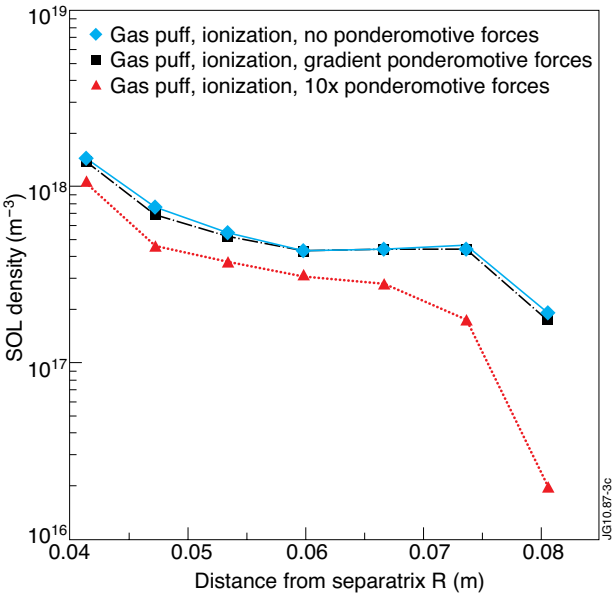


*Figure 21: Effects of the gas puff.*

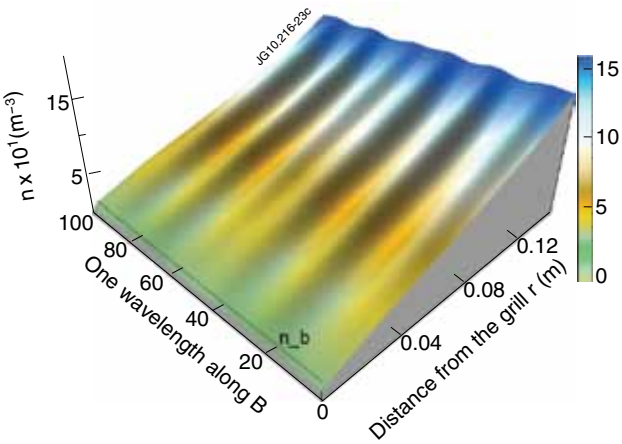


*Figure 22: Graph of density n(r,z) in front of the grill modulated by ponderomotive forces [26] for the LH power flux = 1.86kW/cm$^2$, temperature scale length $L_T$ = 3cm, density scale length $L_n$ = 1cm, temperature in front of the grill T = 20eV, $n_b = 2.4\times10^{17}$ m$^{-3}$.*